ACS APPLIED MATERIALS & INTERFACES

Research Article

www.acsami.org

Aqueous Solution-Phase Selenized $CuIn(S,Se)_2$ Thin Film Solar Cells Annealed under Inert Atmosphere

Yunjung Oh,[†] Wooseok Yang,[†] Jimin Kim,[†] Kyoohee Woo,[‡] and Jooho Moon*[,†]

[†]Department of Materials Science and Engineering, Yonsei University, 50 Yonsei-ro Seodaemun-gu, Seoul 120-749, Republic of Korea

[‡]Advanced Manufacturing Systems Research Division, Korea Institute of Machinery and Materials, 156 Gajeongbuk-ro, Yuseong-gu, Daejeon 305-343, Republic of Korea

Supporting Information

ABSTRACT: A nonvacuum solution-based approach can potentially be used to realize low cost, roll-to-roll fabrication of chalcopyrite $CuIn(S,Se)_2$ (CISSe) thin film solar cells. However, most solution-based fabrication methods involve highly toxic solvents and inevitably require sulfurization and/or postselenization with hazardous H_2S/H_2Se gases. Herein, we introduce novel aqueous-based Cu−In−S and Se inks that contain an amine additive for producing a high-quality absorber layer. CISSe films were fabricated by simple deposition of Cu−In−S ink and Se ink followed by annealing under an inert atmosphere. Compositional and phase analyses confirmed that our simple aqueous ink-based method facilitated in-site selenization of the CIS layer. In addition, we investigated the molecular structures of our aqueous inks to determine how crystalline chalcopyrite absorber layers developed without sulfurization and/or postselenization. CISSe thin film solar cells annealed at 550 °C exhibited an efficiency of 4.55% under AM 1.5 illumination. The low-cost, nonvacuum method to deposit chalcopyrite absorber layers described here allows for safe and simple processing of thin film solar cells.

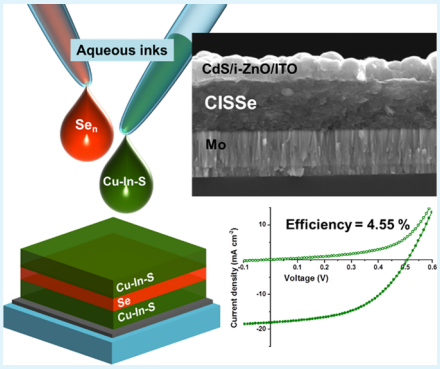

KEYWORDS: *CISSe thin film solar cell, solution processing, solution-phase selenization, complexing agent, inert atmosphere annealing*

1. INTRODUCTION

$Cu(In,Ga)(S,Se)_2$ (CIGSSe) is considered a promising absorber material for thin film photovoltaics due to its high absorption coefficient ($\sim 10^5$ cm^{-1}) with direct band gap, and reduced usage of the toxic element cadmium (as compared to CdTe thin film). In particular, the tunable band gap of these ternary chalcopyrite semiconductors ranges from 1.5 eV ($CuInS_2$ (CIS)) to 1.02 eV ($CuInSe_2$ (CISe)), which matches the solar spectrum well.[1] Most high performance CIGSSe solar cells have been fabricated by vacuum-based deposition methods such as coevaporation and sputtering.[2] However, the high production cost of conventional vacuum processes is a major obstacle to the mass production of CIGSSe thin film solar cells. Many researchers have therefore developed alternative deposition techniques based on nonvacuum processes. Nonvacuum-based solution processes have the potential to lower production costs, which could translate to large-area and high throughput fabrication.[3]

To date, a wide variety of nonvacuum approaches have been utilized to fabricate a high-quality CIGSSe absorber layer. Mitzi et al. reported that CIGSSe thin film solar cells produced by a hydrazine-based solution process had a power conversion efficiency (PEC) of 15.2%.[4] Hydrazine has been used to dissolve Cu_2S, In_2Se_3, as well as S and Se with molecular-level blending constituents so that hydrazine can form metal−chalcogenide networks that can be easily converted into high-quality chalcopyrite structures without any postannealing process.[5,6] Despite the high PEC of these hydrazine-derived CIGSSe thin film solar cells, however, the highly toxic and explosive chemical nature of hydrazine makes it difficult for this strategy to be deployed in practical applications. To fully realize the advantages of a nonvacuum process, nonflammable environmentally benign solvents should be used to produce the high-quality absorber layer. Nontoxic solvent-based processes have been successfully employed to produce CIGSSe layers with a PEC of 8.75−10.7%, which is lower than that of their hydrazine or vacuum-deposited counterparts.[7−10] To produce high-quality absorber layers from nontoxic solvent-based processes, several challenges still remain to be resolved. First, most nontoxic solvents are unable to dissolve S/Se components, which makes it difficult to form uniform metal−chalcogenide networks as are formed when using hydrazine. Thus, postsulfurization and/or selenization processes that require complex instrumentation[11] and extremely toxic gaseous reactions with H_2S/H_2Se are generally used to produce nontoxic solution-processed absorbers.[12,13] Worse, during the post-sulfurization/selenization process, vigorous gaseous reactions occur on the surface of the absorber layer, which usually induces formation of an undesirable double-layered structure consisting of a dense top layer and porous bottom layer or a nonuniform compositional distribution along the depth direction.[14] Second, widely used nontoxic solvents such as

Received: July 30, 2015
Accepted: September 22, 2015
Published: September 22, 2015

DOI: 10.1021/acsami.5b06996
ACS Appl. Mater. Interfaces 2015, 7, 22570−22577

Scheme 1. Schematics Showing Three Different Absorber Layers as a Function of Deposition Sequence and Ink Type[a]

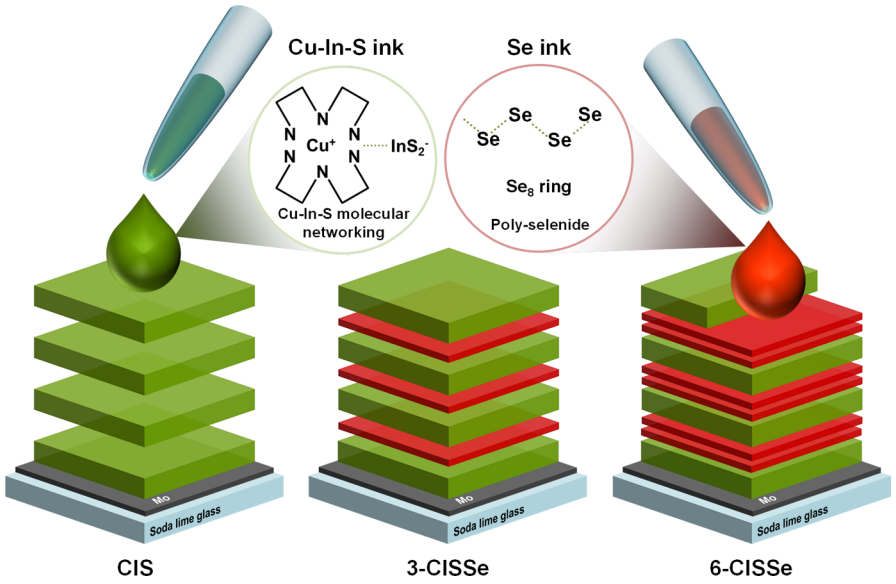

[a]The 3-CISSe film was coated three times with Se ink, whereas the 6-CISSe film was coated six times.

ethanol, dimethyl sulfoxide, and ethylene glycol contain carbon components, which could lead to carbon residues in the absorber layer.[13] In this respect, developing water-based aqueous system that can dissolve S/Se components is a promising approach to realize a high-quality absorber layer without use of toxic solvents or gaseous reactions. Although we successfully synthesized aqueous sol−gel derived CIGS solar cells with a PEC of 7.04%, we used H_2S sulfurization to induce sufficient grain growth.[14] Herein, we report the synthesis of solution-processed $CuIn(S,Se)_2$ (CISSe) solar cells using a simple, nontoxic, green aqueous ink without postselenization or explosive gas reactions. To exclude any gaseous reactions, we directly dissolved the S/Se component in aqueous ink through solution chemistry using an amine additive. We separately prepared aqueous Cu−In−S ink and Se ink to facilitate self-organized "Cu−In−S molecular networking" and poly selenide molecule formation, respectively.[15] Se ink was incorporated in the middle of the CIS absorber layers formed by spin-coating Cu−In−S ink to achieve "solution-phase selenization", resulting in the production of a high-quality CISSe absorber by annealing under inert conditions. Our novel aqueous ink-based approach allows the synthesis of thin film solar cells through safe and readily achievable processes that do not require toxic H_2S/H_2Se gas or S/Se vapor.

2. EXPERIMENTAL SECTION

2.1. CISSe Film Preparation and Device Fabrication. Aqueous Cu−In−S ink was prepared by dissolving appropriate amounts of $Cu(HCO_2)_2{\cdot}4H_2O$ (98%, Alfa Aesar, Heysham, Lancashire, UK), $In(NO_3)_3{\cdot}xH_2O$ (99.9%, Sigma-Aldrich, St. Louis, MO), and S (99.9%, Sigma-Aldrich) in deionized water (DIW) with the amine additive of diethylenetriamine (DETA, 99%, Sigma-Aldrich). The molar ratio of Cu:In:S was 0.9:1:3, and the total concentration of metal precursors was 0.2 M. To provide sodium ions to assist the grain growth of CISSe, sodium formate ($NaHCO_2$, Sigma-Aldrich) was also dissolved in the ink. Aqueous Se ink was separately prepared by dissolving Se powder (99.99%, Sigma-Aldrich) in DIW solvent with DETA. The concentration of Se ink was 0.7 M. The volume ratio of DETA/DIW was 0.1. The Cu−In−S ink was stirred at 95 °C for 12 h to give a dark green colloidal suspension. After being stirred, the ink was heated to 100 °C for 15 min to control the viscosity of ink for spin-coating. The Se ink was stirred at 95 °C for 5 h to yield a red solution. The Cu−In−S precursor ink was spin-coated on Mo-coated soda lime glass substrate to produce absorber layers with a thickness of ∼1.2 μm, followed by preannealing on a hot plate in an ambient atmosphere. Thermal behavior of the Cu−In−S ink was evaluated by thermogravimetric analysis as shown in Figure S1. Cu−In−S ink showed significant weight loss around 300 °C without further weight loss, so the preannealing temperature of Cu−In−S ink was determined to be 300 °C. Preannealed films were denoted as-prepared (ASP) films. The drying temperature of Se ink was set to 210 °C. CIS film was created by spin-coating using Cu−In−S ink four times to create a CIS absorber layer. Se layers were inserted in the middle of the CIS precursor films by spin-coating the Se ink, leading to a multilayered absorber containing Cu, In, S, and Se; these films were denoted CISSe films. Different numbers of Se layers were sandwiched between the CIS layers by varying the number of times deposition was performed. Layers referred to as 3-CISSe and 6-CISSe indicate three and six coatings with Se ink, respectively, as depicted in Scheme 1. ASP films were then annealed in a tube furnace at 550 °C. The annealing process consisted of heating the film to the target temperature under 2.5% H_2/Ar atmosphere, followed by a 30 min hold at 550 °C under Ar atmosphere to convert the precursor films into CIS/CISSe absorbers. The annealed absorber films were processed for solar cell fabrication through deposition of CdS (∼60 nm), RF sputtering of *i*-ZnO (∼50 nm), RF sputtering of ITO (∼200 nm), and thermal evaporation of a patterned Ni/Al grid as the top electrode. The final devices were mechanically scribed into cells with an area of 0.16 cm^2. The current−voltage (I−V) characteristics of aqueous ink-derived CIS/CISSe thin film solar cells were measured both in the dark and under AM 1.5 illumination (1000 W m^{-2}).

2.2. Characterization of CIS/CISSe Films and Solar Cells. Thermogravimetric (TG) analysis of Cu−In−S ink was performed under air flow (150 cc min^{-1}) at a heating rate of 10 °C min^{-1} using a SDT Q600 (TA Instruments). Microstructure of the absorber layers was examined using a field emission scanning electron microscope (FESEM, JSM-6701F, JEOL, Japan) equipped with an energy-dispersive X-ray spectroscopy. Phase evolution of absorber layers was determined by X-ray diffraction (XRD, Ultima IV, Rigaku, Japan) with Cu Kα radiation (λ = 0.15406 nm) and Raman spectroscopy (Lab Ram ARAMIS, Horiba Jobin-Yvon) with an Ar-ion laser beam at an excitation radiation wavelength of 514.5 nm. All XRD results were normalized to the (110) plane of the Mo substrate. Compositional depth profiles were investigated by secondary ion mass spectrometry (SIMS) (K-ALPHA, Thermo Fisher Scientific) using a Cs^+ ion beam. Cell performance and external quantum efficiency (EQE) were analyzed by a solar simulator

DOI: 10.1021/acsami.5b06996
ACS Appl. Mater. Interfaces 2015, 7, 22570−22577

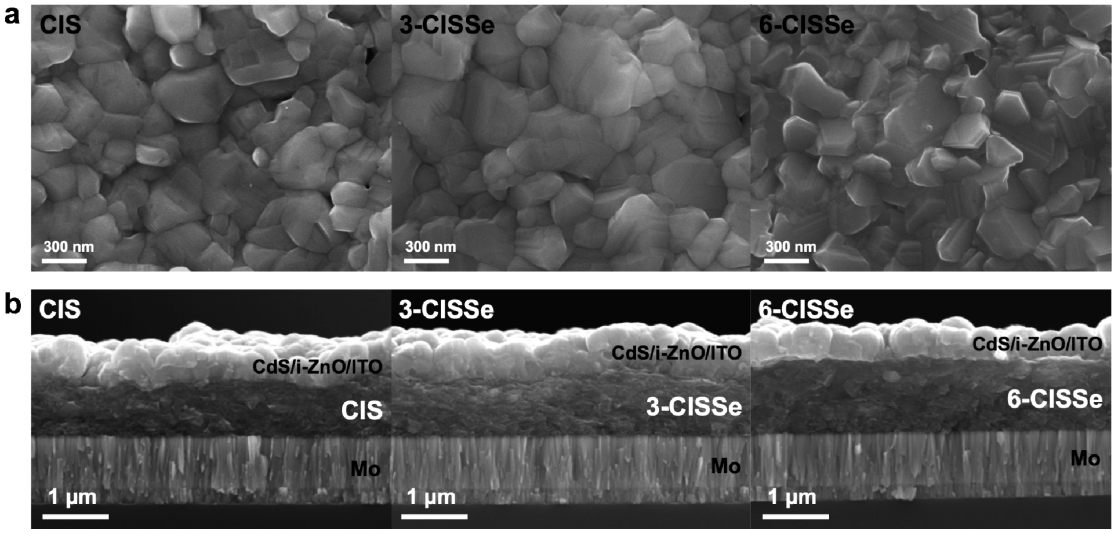

Figure 1. (a) Microstructure evolution of the CIS/CISSe absorber layer. Films were annealed at 550 °C in an Ar atmosphere in a tube furnace. (b) Cross-sectional SEM images of the three devices. All devices were constructed with the configuration of Mo-coated glass/CISSe/CdS/*i*-ZnO/ITO. Thickness of 6-CISSe absorber layer was ∼1.3 μm thick, while the 3-CISSe layer had a thickness of ∼1.2 μm and the CIS layer was ∼1 μm thick. The deviation of the film thickness was ∼0.1 μm.

(Oriel Sol3A Class AAA, Newport Corporation, Irvine, CA) and an incident photon conversion efficiency measurement device (QEX 10, PV Measurements, Inc., Boulder, CO), respectively.

3. RESULTS AND DISCUSSION

Figure 1a shows the surface morphological features of the annealed absorber layers. The surface microstructure of absorber layers changed in appearance after solution-phase selenization. CIS film had a rough surface structure with occasional voids, whereas CISSe film had more faceted grain structures. In addition, the absorber layer adopted a denser grain structure with enlarged fused-like grains as the amount of Se incorporated increased, consistent with previous observations.[8,9] The cross-sectional microstructure of the CIS/CISSe-based thin film solar cells is shown in Figure 1b. The CISSe layers had a smooth surface and uniform grain structure. In particular, the absorber layer of 6-CISSe was the thickness at ∼1.3 μm due to lattice expansion because Se substituted for S in the chalcopyrite crystal structure as a result of solution-phase selenization. Most nontoxic solution-processed CISSe cells require conventional sulfurization/selenization steps in which the gas-phase (H_2S/H_2Se) reaction with the precursor films occurs, in turn leading to a double layered microstructure consisting of a large-grained upper layer and fine-grained bottom layer.[14] Surfaces of the precursor films were exposed to chalcogen sources so that the sulfurization/selenization proceeded from the surface to the bottom. The upper precursor layer first reacted with gaseous reactants, and a crystallized chalcopyrite structure formed at the surface. The densely grown upper layer functioned as a blocking layer that prevented further sulfurization/selenization reactions at the bottom layer, resulting in a double-layered structure. The conventional sulfurization/selenization process leaves carbon impurities in the bottom fine-grained layer.[13] By contrast, the absorber layers fabricated with our aqueous ink were single layer structures without carbon impurities, which will be discussed in more detail later.

The surface composition of the absorber layers was determined by energy-dispersive X-ray spectroscopy (EDX); the results are listed in Table 1. The average metallic compositions of annealed films were close to the initial precursor composition. Se/(Se+S) ratio increased from 0.16 to 0.31 as the number of times Se ink was deposited increased. EDX elemental mapping of the CISSe surface also confirmed that solution-phase selenization could induce uniform distribution of components without aggregation of Se, as shown in Figure S2. SIMS depth profiling was conducted to determine the compositional distribution along the depth direction (Figure 2a). Unlike in the CIS/Mo sample, selenium atoms were detected in the CISSe/Mo sample. In addition, carbon residues were almost absent from the three absorber layers, implying that the preannealing process was sufficient to eliminate carbon impurities. Furthermore, oxygen impurities are also absent in the absorber layer. The relative metallic compositional depth profile (i.e., blue line) indicated that both CIS and CISSe layers had a uniform compositional distribution, as shown in Figure 2b. Cu/In ratios of CIS, 3-CISSe, and 6-CISSe were determined to 0.78, 0.83, and 0.85, respectively, which was close to the initial precursor composition ratio. The average composition ratio of Se/(Se+S) across the depth was 0.14 for 3-CISSe and 0.30 for 6-CISSe, close to the values obtained by EDX analysis. However, the local Se/(Se+S) ratio increased slightly according to depth profiles for both 3-CISSe and 6-CISSe layers. This observation indicates the presence of Se grading in the CISSe layers. Such variation likely results from a nonuniform distribution of chalcogen elements; Se increased slightly and S decreased abruptly toward the bottom of the absorber layer, as shown in Figure 2a. Se segregation at the bottom may have occurred due to repetitive selenium ink coating of porous ASP-CIS film. Surface images of ASP-CIS/CISSe are shown in Figure S3. The ASP-CIS film had a porous microstructure, while ASP-6-CISSe had a

Table 1. Composition Ratio at the Surface of CIS/CISSe Layers As Determined by EDX

	after annealing		
sample ID	Cu/In	(S+Se)/Cu	Se/(S+Se)
CIS	0.94	2.79	0.00
3-CISSe	0.89	2.66	0.16
6-CISSe	0.91	2.48	0.31

DOI: 10.1021/acsami.5b06996
ACS Appl. Mater. Interfaces 2015, 7, 22570−22577

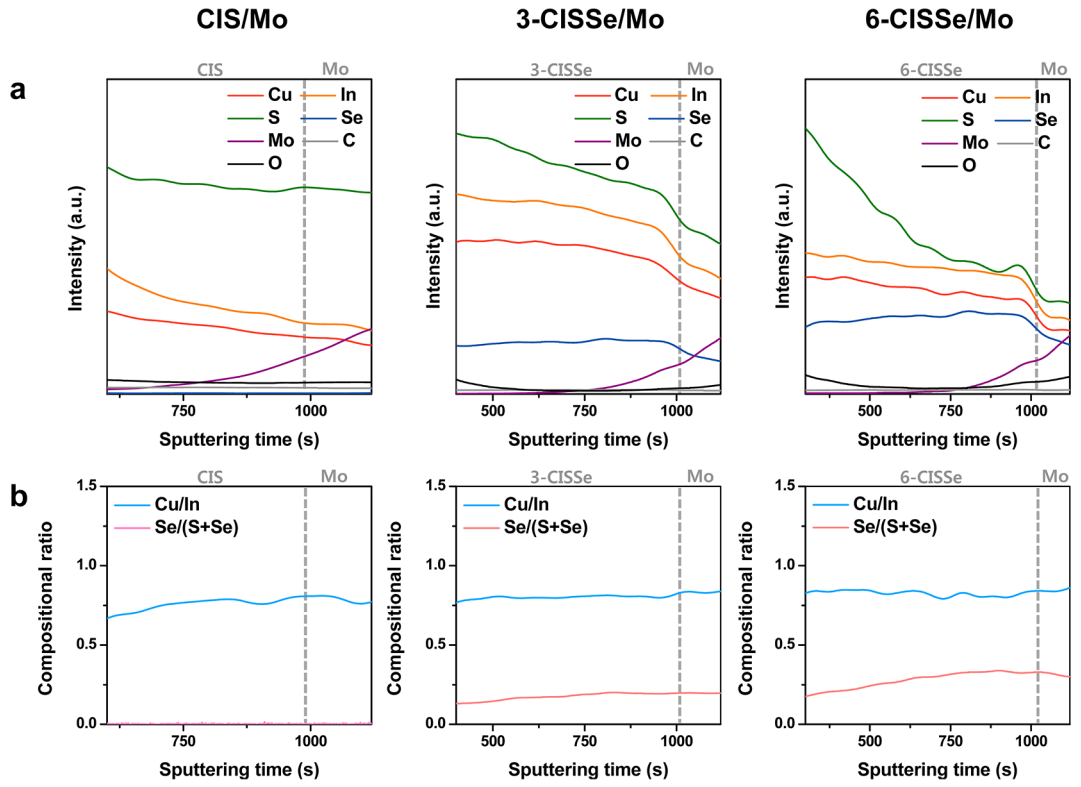

Figure 2. (a) SIMS depth profiles of the absorber layer deposited on the Mo-coated substrate. (b) Compositional ratio along the thickness direction. Cu/In ratio of CIS, 3-CISSe, and 6-CISSe was determined to 0.78, 0.83, and 0.85, respectively.

smoother and denser surface than ASP-3-CISSe. Se ink likely filled the pores of ASP-CIS film during repetitive deposition of Se ink, and eventually capillary force caused the selenium source to segregate at the bottom of the films. Indeed, cross-sectional EDX mapping of ASP-CISSe films revealed that Cu, In, and S were uniformly distributed along the films, while there was slight grading of the Se component (Figure S4). This observation led us to speculate that the decline in S according to film depth was related to its elimination during the annealing process. Se incorporated between the ASP-CIS layers would have substituted for S in the formation of Cu−In−Se-based chalcopyrite. After replacement, the remaining sulfur not incorporated into the chalcopyrite structure would have become volatile during annealing at 550 °C, because the boiling temperature of sulfur is 445 °C, while Se evaporates at 685 °C. For the 6-CISSe layer, the substitution reaction would have occurred significantly more frequently at the bottom where more Se was present than the surface, leading to a more severe sulfur deficiency at the bottom than the 3-CISSe film. Therefore, ASP-CISSe films with initial Se grading were converted into chalcopyrite CISSe films with slight Se grading after annealing as determined by SIMS depth profiling. Despite the Se grading, however, we demonstrated that our solution-phase selenization process allowed for facile, safe, and controllable selenization.

XRD analysis verified the formation of crystalline CIS/CISSe, as shown in Figure 3a. The sharp peaks of the sulfide CIS film at 28.0°, 46.7°, and 55.5° represent diffraction of the (112), (204/220), and (116/312) planes (JCPDS no. 27-0159), indicative of the chalcopyrite structure of $CuInS_2$. The position of the (112) plane of CIS was shifted from 28.02° through 27.96° for 3-CISSe to 27.89° for 6-CISSe because sulfur was replaced with selenium in the chalcopyrite crystal lattice (as shown in enlarged Figure 3a).[6] It is noteworthy that the full-width-at-half-maximum (FHWM) of CISSe film was larger than that of the CIS layer, indicating the possible coexistence of a nonstoichiometric/nonchalcopyrite phase or mixture of phases with different Se/(S+Se) ratios (i.e., Se grading). However, XRD did not have sufficient resolution to clarify the existence of a secondary phase, so we conducted Raman spectroscopy to more closely investigate the phases in our absorber layers. Raman spectrum exhibited a strong A_1 mode for the CIS layer at 291 cm^{-1} (Figure 3b). The A_1 mode represents anion (S or Se) vibrational movement correlated with cations (Cu, In) at rest. We attributed the small peaks at 240, 320, and 340 cm^{-1} to the B/E mode of chalcopyrite $CuInS_2$.[16] Sulfur vibrational peaks of the $CuInS_2$ A_1 mode shifted gradually to 290 cm^{-1} for 3-CISSe and 289 cm^{-1} for 6-CISSe because A_1 vibration was affected by the presence of neighboring Se atoms.[6] The selenium vibrational mode of $CuInSe_2$ A_1 located around 212 cm^{-1} for the CISSe films increased in intensity as the amount of Se incorporated increased (i.e., from 3-CISSe to 6-CISSe).[17−20] The peak of the selenium vibrational mode was significantly red-shifted as compared to the ideal A_1 mode (176 cm^{-1}) of the $CuInSe_2$ phase, because the Raman shift of selenium vibration of $CuInSe_2$ A_1 varies as a function of Se/(Se+S) composition ratio.[20] Meanwhile, all absorber layers retained an undesirable Cu−Au ordered CIS phase at 309 cm^{-1}, but the intensity of this phase decreased with increasing incorporated Se content. On the other hand, Cu−Au ordered CISe phase peaks located at 185 cm^{-1} were not detected for all three samples.[18] Cu−Au ordered CIS is likely present even at room temperature due to its low formation energy.[16] Therefore, we assumed that Cu−Au ordered CIS phase forms from Cu−In−S ink during the preannealing process. After solution-phase selenization, Cu−Au ordered CIS phase transforms to chalcopyrite CISSe phase. All CIS/CISSe absorber layers had a broad A_1 mode, reflecting the relatively poor

DOI: 10.1021/acsami.5b06996
ACS Appl. Mater. Interfaces 2015, 7, 22570−22577

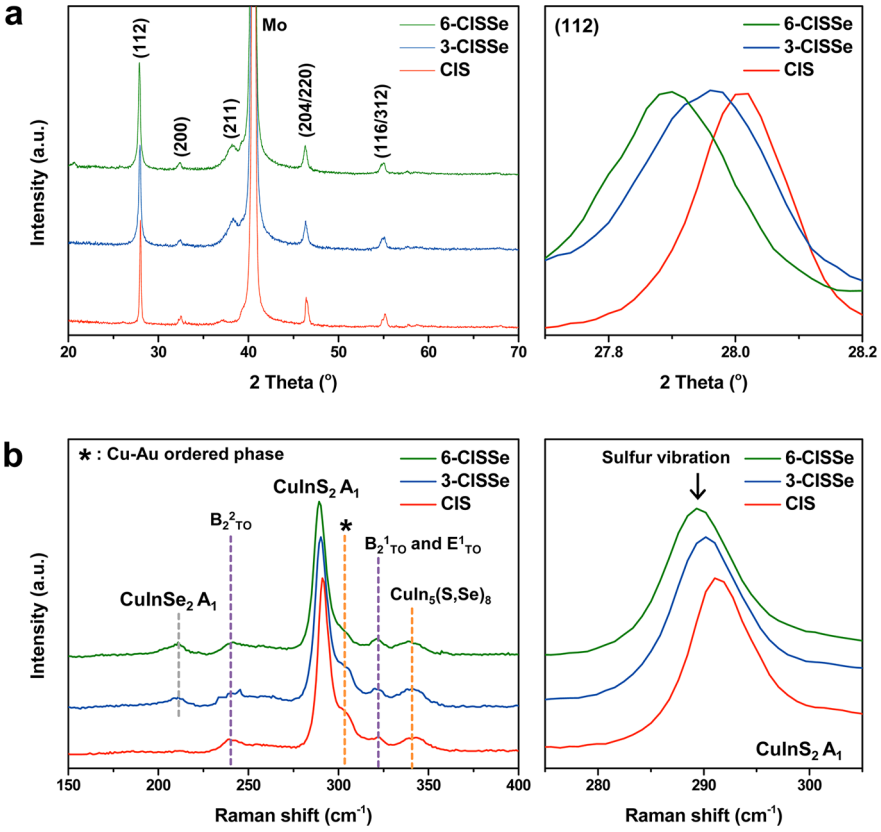

Figure 3. (a) XRD results of CIS/CISSe films fabricated on Mo-coated glass substrate. Enlarged graphs in the 2θ angle range 27.6–28.2° are also displayed. (b) Raman spectra of CIS/CISSe films annealed at 550 °C. Enlarged graphs in the range from 270 to 310 cm^{-1} are also displayed. All thin film layers were annealed under inert conditions.

crystallinity of the chalcopyrite structure. A Cu–Au ordered phase and poor crystallinity could potentially degrade cell performance.[21]

We analyzed the molecular structure of our aqueous inks by Raman spectroscopy to determine the constituent elements present in the aqueous phase and how facile phase formation of chalcopyrite structure and in situ selenization without a gaseous source such as H_2Se or vapor Se were possible. For aqueous Cu–In–S ink, three distinctive peaks at 320, 445, and 475 cm^{-1} were visible, as shown in Figure 4a. The peak located at 320 cm^{-1} was assigned to the In–S stretching mode, while the 450 cm^{-1} peak was attributed to Cu–N stretching vibrations, which might be related to the chelation of Cu^+ by DETA.[22] Furthermore, the peak at 475 cm^{-1} was assigned to vibration of sulfur that is typically bonded with other elements.[23] The S–S stretching mode of sulfur powder was absent (typically the strongest peak at 290 cm^{-1}). Therefore, we assumed that sulfur was present in bonded form as H–S or In–S. Previous studies assigned the S–H stretching mode to the peak at 2530 cm^{-1};[24] this peak was not present in our Cu–In–S ink, as shown in Figure 4b. We therefore assumed that elemental sulfur was bonded with In as In–S. NO_3^- and HCO_2^- anions from the metal precursors were found in the range of 1000–1500 cm^{-1}.[25] On the basis of Raman results, we speculated that DETA acted as both a reducing and a chelating agent in our aqueous ink. DETA can chelate Cu^+ ions to form $[Cu(DETA)_2]^+$, which prevents the formation of binary Cu sulfides and promotes the generation of ternary sulfides. In addition, DETA reduces dissolved elemental S to the S^{2-} anion, followed by reaction with In^{3+} to form InS_2^-.[26] Indium sulfide anions in the ink likely bonded with $[Cu(DETA)_2]^+$ to create a "Cu–In–S molecular network" as depicted in Scheme 1. A network with the unit of $[Cu(DETA)_2]^+$–InS_2^- has a stoichiometric atomic ratio of $CuInS_2$.[26] The ASP film of CIS revealed crystalline chalcopyrite and binary sulfide phases as shown in Figure S5. After preannealing in air, the homogeneously dispersed "molecular network" underwent rearrangement of the Cu–In–S molecular network upon decomposition of DETA and anions. The rearranged Cu–In–S molecular network likely formed chalcopyrite and binary sulfide phases because of their molecular structural similarity. Binary sulfide phase may have resulted from partial segregation of metallic components or insufficient chelation of copper cations. Condensed Cu–In–S network structures in the ASP film would have required less thermal energy for further crystallization, leading to a well-crystallized chalcopyrite structure at 550 °C without the aid of an additional gaseous source. However, the binary sulfide phase formed during the preannealing process likely induced the Cu–Au ordered secondary phase that was detected by Raman spectroscopy, because annealing without any gaseous source might be insufficient to convert binary sulfide into a chalcopyrite structure.

The Raman spectrum of selenium ink is presented in Figure 4c. The most intense peak located at 245 cm^{-1} was attributed to Se–Se vibrations in polymeric selenium chains, while the peak at 275 cm^{-1} was attributed to symmetric Se–Se stretching in the Se_8 cyclic species.[15,27,28] No peak at 2330 cm^{-1}, which corresponds to Se–H stretching vibrations, was present (Figure 4d).[27] Thus, we assumed that elemental selenium dissolved in DIW with the aid of DETA formed poly selenide molecules such as Se_8 rings, as depicted in Scheme 1. In the aqueous Se ink, DETA likely

DOI: 10.1021/acsami.5b06996
ACS Appl. Mater. Interfaces 2015, 7, 22570–22577

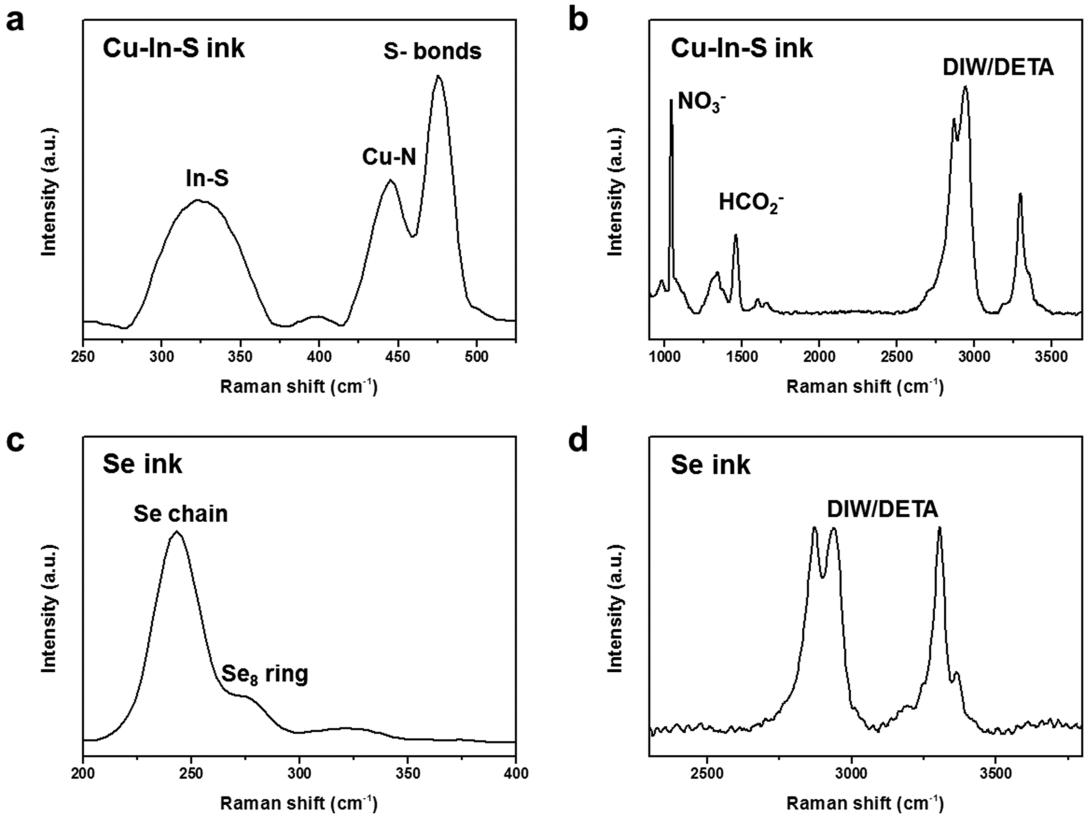

Figure 4. Raman spectra of (a,b) Cu−In−S ink and (c,d) Se ink.

reduced Se to Se^{2-}, and Se^{2-} reacted with other Se atoms to form poly selenide molecules through polymerization.[15] These poly selenide molecules were deposited in the form of Se ink between the ASP-CIS layers, allowing for solution-phase selenization. The deposited poly selenide molecules might have acted as fluxing agents, leading to liquid-phase-assisted selenization during annealing under an inert atmosphere.[29] The solution-phase selenization reaction resulted in substitution of Se for S to form a chalcopyrite condensed Cu−In−S network. As shown in Figure 1, CISSe film, which was accompanied by volumetric expansion, had dense and fused grain microstructures as compared to those of CIS films. In addition, the phase analysis shown in Figure 3b indicated that the Cu−Au ordered phase decreased as the amount of Se ink increased. This observation indicated that the liquid-phase-assisted reaction by poly selenide molecules promoted the crystallization of chalcopyrite structures.

Aqueous ink-based thin film solar cells were constructed in the following configuration: Mo-coated glass/CIS(Se)/CdS/*i*-ZnO/ITO/Ni/Al without an antireflection layer. According to the current density−voltage (J−V) characteristics, the 6-CISSe-based device had the highest efficiency of 4.55%, with an open-circuit voltage (V_{OC}) of 0.51 V, a short circuit current density (J_{SC}) of 18.06 mA cm^{-2}, and a fill factor (FF) of 49.61% as shown in Figure 5a. The performance parameters of the CIS/CISSe devices are listed in Table 2. To demonstrate the reproducibility of our solar cells, the performance statistics of 10 devices made using each of the three film types are shown in Figure S6. While all devices exhibited stable performance parameters without appreciable degradation, the device parameter values of the CIS solar cell were inferior to those of its CISSe counterpart. Current density increased with enhanced Se content, as did V_{OC}. The improvement in current density was induced by a reduction in the band gap upon selenization. The low efficiency of CIS solar cells has several causes. As shown in Figure 1a, the CIS absorber layer had a small grain size and voids, which induced rough interface contacts with the buffer/TCO layer, resulting in a decrease in FF.[30] The occasional voids in the CIS solar cell induced interfacial resistance between CdS−CIS heterojunctions. In addition, recombination loss through dangling bonds at the grain boundaries may have decreased the open circuit voltage. Raman spectroscopy showed that the level of impurities in CIS was higher than that in the selenide absorber layers, as determined by the higher intensity of the Cu−Au ordered phase in the former as shown in Figure 3b. In the same manner, 3-CISSe films have more Cu−Au ordered phase than 6-CISSe, resulting in a decrease in V_{OC}.[16]

Figure 5b shows the external quantum efficiency (EQE) of the CIS/CISSe devices. The 6-CISSe devices showed a maximum quantum efficiency of 67% at 550 nm. For the CIS device, there was significant drop in the EQE response in the shorter wavelength region, leading to a reduction in J_{SC}. We ascribed the quantum efficiency loss in the short wavelength range below ~500 nm to absorption in the buffer layer. For the CISSe devices, a broad middle band response and a sharp tail toward the band gap cutoff indicated suitable carrier collection.[31] The band gap was determined by fitting a plot of $[E \ln(1 - \mathrm{EQE})]^2$ versus E near the band edge as shown in Figure S7 and Table 2. The band gap of the CIS layer was smaller than the ideal band gap (1.55 eV) of CIS; the secondary phase might have lowered the band gap of our film, as discussed in Figure 3b.[32] However, 3-CISSe and 6-CISSe layers had band gaps in the range of 1.40−1.49 and 1.36−1.46 eV, respectively, suggesting that the CISSe absorber layers had compositional Se grading along the depth direction as determined by SIMS depth profiles. The relatively low quantum

DOI: 10.1021/acsami.5b06996
ACS Appl. Mater. Interfaces 2015, 7, 22570−22577

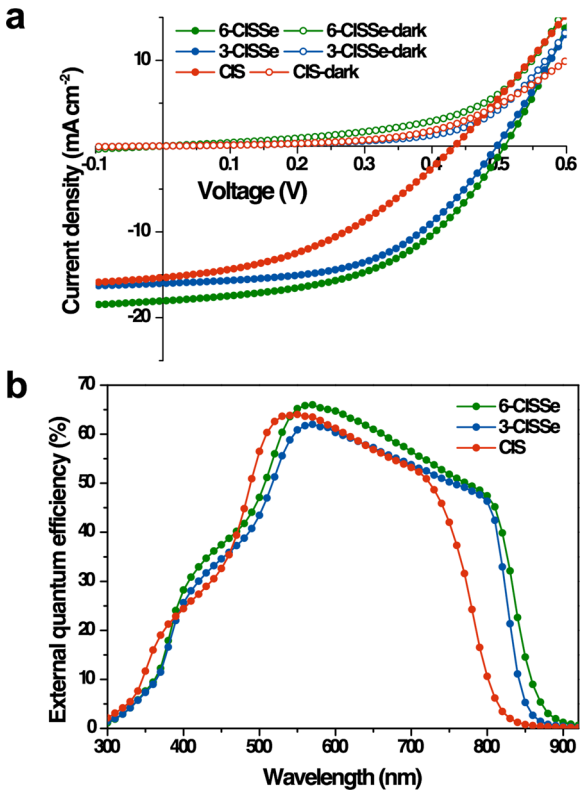

Figure 5. (a) Current density−voltage (J−V) characteristics of CISSe solar cells annealed at 550 °C. The closed solid mark represents the J−V curve under 1.5 illumination, whereas the open mark stands for currents measured in the dark. (b) External quantum efficiency (EQE) curves of CIS, 3-CISSe, and 6-CISSe devices. The 6-CISSe device has a current density of 16.9 mA cm^{-2} calculated on the basis of EQE results.

Table 2. Device Performance of CIS/CISSe Solar Cells Annealed at 550 °C under Inert Conditions

sample ID	V_{OC} (V)	J_{SC} (mA cm^{-2})	FF (%)	η (%)	band gap (eV)[a]
CIS	0.43	15.25	41.11	2.72	1.52
3-CISSe	0.49	15.98	52.41	4.16	1.40
6-CISSe	0.51	18.06	49.61	4.55	1.36

[a]The band gap of the absorber layer was determined by fitting of $[E\ \ln(1 - \mathrm{EQE})]^2$ versus E near the band edge as shown in Figure S7.

efficiency of CISSe resulted from Se-grading in the absorber layer. The Se-rich bottom would have induced a slight increase in the valence band and significantly decreased the conduction band, which may have improved majority carrier collection at the back contact and caused poor carrier diffusion of electrons,[33] resulting in a low current density.

Although the efficiency of our CIS/CISSe cells was lower than those of other cells produced by nontoxic solution process with H_2S sulfurization or postselenization,[7−11] improvements in device performances are expected after further studies to resolve several issues. One of the possible reasons for the relatively low efficiencies is the presence of small-sized grains and secondary phase resulting from insufficient crystallization of the chalcopyrite structure. Actually, in many reported works, chalcogenide thin film solar cells with small grain size tend to exhibit low efficiency because many grain boundaries in small-grained layer can behave as charge trapping sites, inducing recombination of carriers and increasing series resistance.[14,35] In this sense, we expect that higher efficiency can be achieved by increasing the grain size and removing secondary phases with further optimization of the annealing process. Furthermore, the slight Se grading present in our absorber layer is another possible reason for the low cell efficiency. Ink properties (e.g., concentration) and coating methods need to be modified to control the porosity of ASP-CIS to induce uniform selenium distribution along the depth direction of the absorber layer. Moreover, band gap grading, such as "normal-graded" or "V-graded", may enhance carrier collection by the thin film solar cells and can be developed by adjusting the stacking sequence of aqueous inks.[34] Finally, incorporation of an antireflection layer might improve cell efficiency. Despite the relatively low efficiency of our devices, the device efficiency is one of the highest reported for chalcopyrite solar cells fabricated without a sulfurization and postselenization process, and represents the first attempt to utilize in situ solution-phase selenization based on aqueous ink. We believe that resolving these issues will enable the production of large area, low cost, all-solution processed CISSe solar cells with high efficiencies.

4. CONCLUSIONS

In summary, our simple aqueous-based deposition approach allowed the synthesis of high-quality CIS/CISSe thin film solar cells. Aqueous Cu−In−S ink containing an amine additive was readily achievable without the involvement of a complex particle synthesis step and highly toxic solvents. Cu−In−S molecular network could be transformed to compositionally uniform CIS absorber layers by annealing, and in situ solution-phase selenization was accomplished successfully using aqueous Se ink. The resulting CISSe thin-film solar cells had a maximum power conversion efficiency of 4.55% (V_{OC} = 0.51 V, J_{SC} = 18.06 mA cm^{-2}, FF = 46.61%) when annealed at 550 °C, which is the highest value reported to date for nontoxic solvent-based CISSe cells without any toxic and explosive gaseous reactions. Our simple, green fabrication method represents a step forward in the realization of nonvacuum ink-based selenization.

■ ASSOCIATED CONTENT

Supporting Information

The Supporting Information is available free of charge on the ACS Publications website at DOI: 10.1021/acsami.5b06996.

TG analysis of Cu−In−S ink, EDX mapping of CISSe thin films, cross-sectional EDX mapping of CISSe solar cells and ASP-CISSe, SEM images of ASP-CIS/ASP-CISSe, XRD showing the phase analysis of ASP-CIS film, calculation of band gap through fitting of a plot of $[E\ \ln(1 - \mathrm{EQE})]^2$ versus E near the band edge, and statistical analysis of CIS/CISSe device parameters (PDF)

■ AUTHOR INFORMATION

Corresponding Author

*Tel.: +82-2-2123-2855. Fax: +82-2-312-5375. E-mail: jmoon@yonsei.ac.kr.

Notes

The authors declare no competing financial interest.

■ ACKNOWLEDGMENTS

This work was supported by a grant from the National Research Foundation (NRF) of Korea funded by the Korean government (MSIP) (no. 2012R1A3A2026417).

DOI: 10.1021/acsami.5b06996
ACS Appl. Mater. Interfaces 2015, 7, 22570−22577

REFERENCES

(1) Hibberd, C. J.; Chassaing, E.; Liu, W.; Mitzi, D. B.; Lincot, D.; Tiwari, A. N. Non-Vacuum Methods for Formation of Cu (In, Ga) (Se, S)$_2$ Thin Film Photovoltaic Absorbers. *Prog. Photovoltaics* **2010**, *18*, 434−452.

(2) Chirilă, A.; Buecheler, S.; Pianezzi, F.; Bloesch, P.; Gretener, C.; Uhl, A. R.; Fella, C.; Kranz, L.; Perrenoud, J.; Seyrling, S. Highly Efficient Cu(In,Ga)Se2 Solar Cells Grown on Flexible Polymer Films. *Nat. Mater.* **2011**, *10*, 857−861.

(3) Habas, S. E.; Platt, H. A.; Van Hest, M. A. F.; Ginley, D. S. Low-Cost Inorganic Solar Cells: from Ink to Printed Device. *Chem. Rev.* **2010**, *110*, 6571−6594.

(4) Todorov, T. K.; Gunawan, O.; Gokmen, T.; Mitzi, D. B. Solution-Processed Cu(In, Ga)(S, Se)$_2$ Absorber Yielding a 15.2% Efficient Solar Cell. *Prog. Photovoltaics* **2013**, *21*, 82−87.

(5) Chung, C.-H.; Li, S.-H.; Lei, B.; Yang, W.; Hou, W. W.; Bob, B.; Yang, Y. Identification of the Molecular Precursors for Hydrazine Solution Processed CuIn (Se, S)$_2$ Films and Their Interactions. *Chem. Mater.* **2011**, *23*, 964−969.

(6) Chung, C.-H.; Lei, B.; Bob, B.; Li, S.-H.; Hou, W. W.; Duan, H.-S.; Yang, Y. Mechanism of Sulfur Incorporation into Solution Processed CuIn (Se, S)$_2$ films. *Chem. Mater.* **2011**, *23*, 4941−4946.

(7) Park, S. J.; Cho, J. W.; Lee, J. K.; Shin, K. S.; Kim, J. H.; Min, B. K. Solution Processed High Band-gap $CuInGaS_2$ Thin Film for Solar Cell Applications. *Prog. Photovoltaics* **2014**, *22*, 122−128.

(8) Septina, W.; Kurihara, M.; Ikeda, S.; Nakajima, Y.; Hirano, T.; Kawasaki, Y.; Harada, T.; Matsumura, M. Cu (In, Ga)(S, Se)$_2$ Thin Film Solar Cell with 10.7% Conversion Efficiency Obtained by Selenization of the Na-Doped Spray-Pyrolyzed Sulfide Precursor Film. *ACS Appl. Mater. Interfaces* **2015**, *7*, 6472−6479.

(9) Hossain, M. A.; Tianliang, Z.; Keat, L. K.; Xianglin, L.; Prabhakar, R. R.; Batabyal, S. K.; Mhaisalkar, S. G.; Wong, L. H. Synthesis of Cu (In, Ga)(S, Se)$_2$ Thin Films Using an Aqueous Spray-Pyrolysis Approach, and Their Solar Cell Efficiency of 10.5%. *J. Mater. Chem. A* **2015**, *3*, 4147−4154.

(10) Luo, P.; Liu, Z.; Ding, Y.; Cheng, J. A Novel Non-Vacuum Process for the Preparation of CuIn(Se,S)$_2$ Thin-Film Solar Cells from Air-Stable, Eco-Friendly, Metal Salts Based Solution Ink. *J. Power Sources* **2015**, *274*, 22−28.

(11) Uhl, A. R.; Fuchs, P.; Rieger, A.; Pianezzi, F.; Sutter-Fella, C. M.; Kranz, L.; Keller, D.; Hagendorfer, H.; Romanyuk, Y. E.; LaMattina, F.; Yoon, S.; Karvonen, L.; Magorian-Friedlmeier, T.; Ahlswede, E.; VanGenechten, D.; Stassin, F.; Tiwari, A. N. Liquid-Selenium-Enhanced Grain Growth of Nanoparticle Precursor Layers for $CuInSe_2$ Solar Cell Absorbers. *Prog. Photovoltaics* **2015**, *23*, 1110.

(12) Kapur, V. K.; Bansal, A.; Le, P.; Asensio, O. I. Non-Vacuum Processing of $CuIn_{1-x}Ga_xSe_2$ Solar Cells on Rigid and Flexible Substrates Using Nanoparticle Precursor Inks. *Thin Solid Films* **2003**, *431*, 53−57.

(13) Uhl, A. R.; Fella, C.; Chirilă, A.; Kaelin, M. R.; Karvonen, L.; Weidenkaff, A.; Borca, C. N.; Grolimund, D.; Romanyuk, Y. E.; Tiwari, A. N. Non-vacuum Deposition of Cu(In, Ga)Se_2 Absorber Layers from Binder Free, Alcohol Solutions. *Prog. Photovoltaics* **2012**, *20*, 526−533.

(14) Oh, Y.; Woo, K.; Lee, D.; Lee, H.; Kim, K.; Kim, I.; Zhong, Z.; Jeong, S.; Moon, J. Role of Anions in Aqueous Sol−Gel Process Enabling Flexible Cu(In, Ga)S_2 Thin-Film Solar Cells. *ACS Appl. Mater. Interfaces* **2014**, *6*, 17740−17747.

(15) Yannopoulos, S. N.; Andrikopoulos, K. S. Raman Scattering Study on Structural and Dynamical Features of Noncrystalline Selenium. *J. Chem. Phys.* **2004**, *121*, 4747−4758.

(16) Camus, C. *Doktor der Naturwissenschaften*; Freie Universitat: Berlin, 2008.

(17) Theodoropoulou, S.; Papadimitriou, D.; Rega, N.; Siebentritt, S.; Lux-Steiner, M. C.; Raman. and Photoreflectance Study of $CuIn_{1-x}Ga_xSe_2$ Epitaxial Layers. *Thin Solid Films* **2006**, *511*, 690−694.

(18) Tanino, H.; Maeda, T.; Fujikake, H.; Nakanishi, H.; Endo, S.; Irie, T. Raman Spectra of $CuInSe_2$. *Phys. Rev. B: Condens. Matter Mater. Phys.* **1992**, *45*, 13323−13330.

(19) Rincon, C.; Ramirez, F. J. Lattice Vibrations of $CuInSe_2$ and $CuGaSe_2$ by Raman Microspectrometry. *J. Appl. Phys.* **1992**, *72*, 4321−4324.

(20) Bacewicz, R.; Gebicki, W.; Filipowicz, J. Raman Scattering in $CuInS_{2x}Se_{2(1-x)}$ Mixed Crystals. *J. Phys.: Condens. Matter* **1994**, *6*, L777−L780.

(21) Guo, Q.; Ford, G. M.; Yang, W. C.; Walker, B. C.; Stach, E. A.; Hillhouse, H. W.; Agrawal, R. Fabrication of 7.2% Efficient CZTSSe Solar Cells Using CZTS Nanocrystals. *J. Am. Chem. Soc.* **2010**, *132*, 17384−17386.

(22) Helios, K.; Wysokiński, R.; Pietraszko, A.; Michalska, D. Vibrational Spectra and Reinvestigation of the Crystal Structure of a Polymeric Copper (II)−Orotate Complex,$[Cu\ (\mu\text{-}HO_r)(H_2O)_2]_n$: The Performance of New DFT Methods, M06 and M05-2X, in Theoretical Studies. *Vib. Spectrosc.* **2011**, *55*, 207−215.

(23) Ward, A. T. Raman Spectroscopy of Sulfur, Sulfur-Selenium, and Sulfur-Arsenic Mixtures. *J. Phys. Chem.* **1968**, *72*, 4133−4139.

(24) Ozaki, Y.; Mizuno, A.; Itoh, K.; Iriyama, K. Inter-and Intramolecular Disulfide Bond Formation and Related Structural Changes in the Lens Proteins. A Raman Spectroscopic Study in vivo of Lens Aging. *J. Biol. Chem.* **1987**, *262*, 15545−15551.

(25) Socrates, G. *Infrared and Raman Characteristic Group Frequencies: Tables and Charts*; John Wiley & Sons: New York, 2004.

(26) Shi, L.; Yin, P.; Wang, L.; Qian, Y. Fabrication of Single-Crystalline $CuInS_2$ Nanowires Array via a Diethylenetriamine-Thermal Routs. *CrystEngComm* **2012**, *14*, 7217−7221.

(27) Nagata, K.; Ishikawa, T.; Miyamoto, Y. Raman Spectrum of Selenium Dissolved in an Aqueous Solution of Sodium Sulfide. *Jpn. J. Appl. Phys.* **1985**, *24*, 1171−1173.

(28) Laitinen, R.; Steudel, R. Vibrational Spectroscopic Investigations of S_nSe_{8-n} Molecules. *J. Mol. Struct.* **1980**, *68*, 19−32.

(29) Kwon, O. H. Liquid-Phase Sintering. *Mater. Sci. Technol.* **1996**, DOI: 10.1002/9783527603978.mst0199.

(30) Leite, M. S.; Abashin, M.; Lezec, H. J.; Gianfrancesco, A.; Talin, A. A.; Zhitenev, N. B. Nanoscale Imaging of Photocurrent and Efficiency in CdTe Solar Cells. *ACS Nano* **2014**, *8*, 11883−11890.

(31) Chopra, K. L.; Paulson, P. D.; Dutta, V. Thin-film Solar Cells: an Overview. *Prog. Photovoltaics* **2004**, *12*, 69−92.

(32) Riedle, T. *Raman Spectroscopy for the Analysis of Thin $CuInS_2$ Films*, 2002.

(33) Jaffe, J. E.; Zunger, A. Electronic Structure of the Ternary Chalcopyrite Semiconductors $CuAlS_2$, $CuGaS_2$, $CuInS_2$, $CuAlSe_2$, $CuGaSe_2$ and $CuInSe_2$. *Phys. Rev. B: Condens. Matter Mater. Phys.* **1983**, *28*, 5822−5847.

(34) Contreras, M. A.; Tuttle, J.; Gabor, A.; Tennant, A.; Ramanathan, K.; Asher, S.; Franz, A.; Keane, J.; Wang, L.; Noufi, R. High Efficiency Graded Bandgap Thin-Film Polycrystalline Cu(In,Ga)Se_2-Based Solar Cells. *Sol. Energy Mater. Sol. Cells* **1996**, *41*, 231−246.

(35) Zhou, H.; Hsu, C. J.; Hsu, W. C.; Duan, H. S.; Chung, C. H.; Yang, W.; Yang, Y. Non-Hydrazine Solutions in Processing CuIn(S,Se)$_2$ Photovoltaic Devices from Hydrazinium Precursors. *Adv. Energy Mater.* **2013**, *3*, 328−336.

DOI: 10.1021/acsami.5b06996
ACS Appl. Mater. Interfaces 2015, 7, 22570−22577